



## Pilot test and optimization of plasma based deNOx

Stamate, Eugen; Chen, Weifeng; Michelsen, Poul

*Publication date:*  
2009

*Document Version*  
Publisher's PDF, also known as Version of record

[Link back to DTU Orbit](#)

*Citation (APA):*  
Stamate, E., Chen, W., & Michelsen, P. (2009). *Pilot test and optimization of plasma based deNOx*. Danmarks Tekniske Universitet, Risø Nationallaboratoriet for Bæredygtig Energi. Denmark. Forskningscenter Risoe. Risoe-R No. 1689(EN)

---

### General rights

Copyright and moral rights for the publications made accessible in the public portal are retained by the authors and/or other copyright owners and it is a condition of accessing publications that users recognise and abide by the legal requirements associated with these rights.

- Users may download and print one copy of any publication from the public portal for the purpose of private study or research.
- You may not further distribute the material or use it for any profit-making activity or commercial gain
- You may freely distribute the URL identifying the publication in the public portal

If you believe that this document breaches copyright please contact us providing details, and we will remove access to the work immediately and investigate your claim.

# Pilot test and optimization of plasma based deNO<sub>x</sub>

Risø-R-Report

Eugen Stamate, Weifeng Chen and Poul Kerff Michelsen  
Risø-R-1689(EN)  
April 2009



**Authors:** Eugen Stamate, Weifeng Chen and Poul Kerff Michelsen  
**Title:** Pilot test and optimization of plasma based NO<sub>x</sub> reduction  
**Division:** Plasma Physics and Technology Programme

**Risø-R-1689(EN)**  
**April 2009**

**Abstract:**

The NO<sub>x</sub> reduction of flue gas by plasma generated ozone was investigated in pilot test experiments at two industrial power plants running on natural gas (Ringsted) and biomass (Haslev). Reduction rates higher than 95% have been achieved for a molar ratio O<sub>3</sub>:NO<sub>x</sub> of 1.56. Fourier transform infrared and ultraviolet absorption spectroscopy were used for spatial measurements of stable molecules and radicals along the reduction reactor. Reactions of O<sub>3</sub> injected in the flue gas in the reduction reactor were also modeled including the influence of the flue gas temperature, water droplets and SO<sub>x</sub> and HCl content. Experiments are in good agreement with numerical simulations. An optimized oxidation scheme for NO<sub>x</sub> reduction processes with time dependent combustion, such as the biomass power plants, was developed. Ozone production by micro-hollow and capillary discharges at atmospheric pressures was investigated for oxygen and air gas flows.

**ISSN 0106-2840**  
**ISBN 978-87-550-3744-1**

**Contract no.:**

**PSO: 2006-1-6365**

**Group's own reg. no.:**  
**1710047-1**

**Sponsorship:**

**Cover :**

**Pages: 31**  
**Tables: 2**  
**References: 21**

Information Service Department  
Risø National Laboratory for  
Sustainable Energy  
Technical University of Denmark  
P.O.Box 49  
DK-4000 Roskilde  
Denmark  
Telephone +45 46774004  
[bibl@risoe.dk](mailto:bibl@risoe.dk)  
Fax +45 46774013  
[www.risoe.dtu.dk](http://www.risoe.dtu.dk)

# Contents

- 1 Summary
- 2 Pilot test measurements at a power plant running on natural gas
  - 2.1 Introduction
  - 2.2 Experimental details- Ringsted
  - 2.3 Chemical mechanism  $O_3$ - $NO_x$
  - 2.4 Gas phase reactions
  - 2.5 Heterophase reactions
  - 2.6 Hydrolysis of  $N_2O_5$  on droplets
  - 2.7 Results and discussion - Ringsted
  - 2.8 Conclusion – natural gas power plant
- 3 Pilot test measurements at a power plant running on biomass
  - 3.1 Introduction
  - 3.2 Chemical kinetics of  $NO_x$  reduction in the presence of  $SO_x$  and HCL
  - 3.3 Experimental details - Haslev
  - 3.4 Results and discussion
  - 3.5 Conclusion – biomass power plant
- 4 References

## Preface

This report summarizes the work performed by Risø DTU for the PSO project no. 2006-1-6365 “Pilot test and optimization of plasma based NO<sub>x</sub> reduction”.

The project was carried out in collaboration between Risø National Laboratory for Sustainable Energy, Technical University of Denmark (Risø DTU), the Danish Gas Technology Centre (DGC) and DONG Energy over a three year period (March 2006-February 2009). Laboratory experiments on NO<sub>x</sub> reduction and ozone optimization were carried at DGC in collaboration with Risø DTU. The pilot test experiments were carried out at the power plant running on natural gas in Ringsted and at the power plant running on biomass in Haslev.

The authors express their gratitude to Dr. Alexander Fateev for direct support and to Dr. B. Stenum†, Dr. H. Mortensen, Dr. Y. Kusano, Dr. F. Leipold and Dr. H. Bindslev for their early involvement in this research.

## 1 Summary

The aim of the project was to,

- Scale-up of the plasma based NO<sub>x</sub> reduction to pilot scale and test it in a natural gas engine power plant and a biomass power plant;
- Investigate the influence of the additional constituents of flue gas coming from biomass combustion (HCl and SO<sub>2</sub>) and their reaction products collected in the scrubber;
- Develop a chemical kinetics model of plasma based NO<sub>x</sub> reduction;
- Optimise the ozone production using plasma discharges at atmospheric pressure.

All project objectives have been successfully addressed in a very good collaboration between DONG Energy, DGC and Risø DTU. Risø DTU's effort was mainly concentrated on process diagnostics by UV and FTIR during the pilot test measurements, chemical kinetics modelling of the NO<sub>x</sub> reduction process and ozone production optimization.

FTIR and UV gas absorption measurements have been performed during the NO<sub>x</sub> reduction process both at Ringsted (natural gas power plant) and Haslev (biomass power plant). Reduction rates higher than 95% have been achieved for a molar ratio O<sub>3</sub>:NO<sub>x</sub> = 1.56 for the natural gas plant. A rate equation model has been developed to assess the chemical kinetics for the NO<sub>x</sub> process in the reactor under various experimental conditions (for example, different flue gas temperatures and humidity). A good agreement was found between measured and calculated values of the main species. Simulation suggests that in current experiment conditions, the deNO<sub>x</sub> efficiency is highest for a flue gas temperature of 100 °C. The addition of small water spray droplets in the reactor may further improve the NO<sub>x</sub> oxidation rate. Due to combustion particularities in the biomass power plant the NO<sub>x</sub> level exhibited very large variation within time intervals of less than a minute. An optimized reduction scheme that can significantly improve the ozone consumption in a time dependent process has been developed and partially implemented. Kinetic simulations show that SO<sub>2</sub> oxidation by ozone is too low and that HCl and SO<sub>x</sub> are not affecting the NO<sub>x</sub> reduction rate. It was shown that fine water droplets of a few tens of μm contribute significantly to N<sub>2</sub>O<sub>5</sub> capture in the reactor. The ozone production by multi hollow and capillary discharges was investigated for different discharge parameters. The results show that a complex construction structure including thick metallic films deposited on dielectric materials is necessary for long and steady operation of these discharges.

## **2 Pilot test measurements in a power plant running on natural gas**

### ***2.1 Introduction***

Nitrogen oxides ( $\text{NO}_x = \text{NO} + \text{NO}_2$ ) formed during fuel burning affect the quality of air, soil and water through acid rains. At higher concentrations they may also have a direct negative influence on human health [1]. Recent environmental concerns lead to stringent regulations on the allowed levels of  $\text{NO}_x$  emission from combustion power plants, gas turbines, incinerators, boilers, diesel engines and other polluting sources. Available technologies for  $\text{NO}_x$  reduction includes: selective catalytic reduction [2], selective non-catalytic reduction [3, 4], low-temperature oxidation by ozone [5], non-thermal plasma [6-9], electron beam irradiation and several hybrid techniques [10, 11]. Despite of this variety, none of these methods is free of trade-offs and limitations including capital investments and/or operational costs. Low temperature oxidation (LTO) of  $\text{NO}_x$  by ozone ( $\text{O}_3$ ) injection is an attractive gas cleaning process where the relatively insoluble  $\text{NO}_x$  is oxidized to higher oxides such as  $\text{N}_2\text{O}_5$  that are highly soluble and can easily be removed in wet scrubbers [5, 12].  $\text{NO}_x$  oxidation method by ozone injection has several advantages compared to other de $\text{NO}_x$  techniques, as e.g. direct ozone production in the reactor, because the plasma discharge is kept clean and the removal rate of NO is higher than direct oxidation methods where the reverse reactions occur to reform NO and  $\text{NO}_2$  by O radical. [13, 14] Despite of these advantages the low-temperature oxidation technique is still relatively expensive, a fact that requires further process optimization and cost estimation for the whole de $\text{NO}_x$  reduction process. There are only few reports in the literature on  $\text{NO}_x$  reduction experiments on industrial power plants using the LTO technique [15]. Therefore, detailed online measurements of the spatial  $\text{NO}_x$  and ozone concentration profiles along an LTO oxidation reactor will be beneficial for a deeper understanding of the chemical kinetics in order to design an efficient de $\text{NO}_x$  reactor for practical application of LTO technique in industry.

### ***2.2 Experimental details - Ringsted***

The movable measurement stand realized and tested at Risø DTU to collect UV and FTIR data at different port along the reactor is presented in Fig. 1 (a) located at Risø DTU, (b) placed under the reactor inside of the container, (c) including placement details for the optical tables supporting the UV and FTIR equipment.

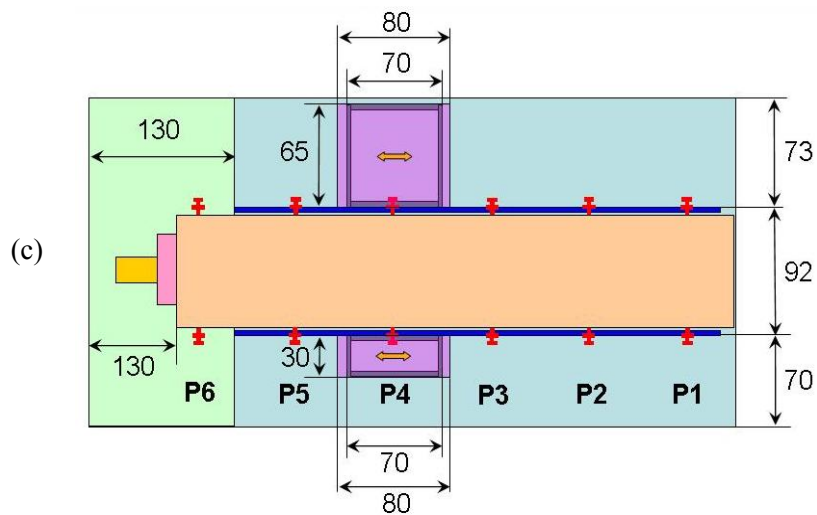


Fig. 1 (a) Movable stand used for UV and FTIR measurements build and tested at Risø DTU; (b) The movable measurement stand placed under the reactor inside of container; (c) Emplacement of the measurements parts near the reactor.



The flue gas source located in Ringsted is a  $2 \times 5.5 \text{ MW}_{\text{el}}$  natural gas fired power plant with a total flow rate of the flue gas of  $49000 \text{ Nm}^3/\text{h}$  from which only a portion of 3% was treated for  $\text{NO}_x$  reduction. The flue gas temperature was steady at  $60^\circ\text{C}$ . The main component of  $\text{NO}_x$  in the flue gas was NO (over 90%) and the total  $\text{NO}_x$  level was kept by process optimization at around 80 ppm. Fig. 2 shows a schematic of the experimental setup. A 4.5 m long and 0.6 m in diameter reactor with a

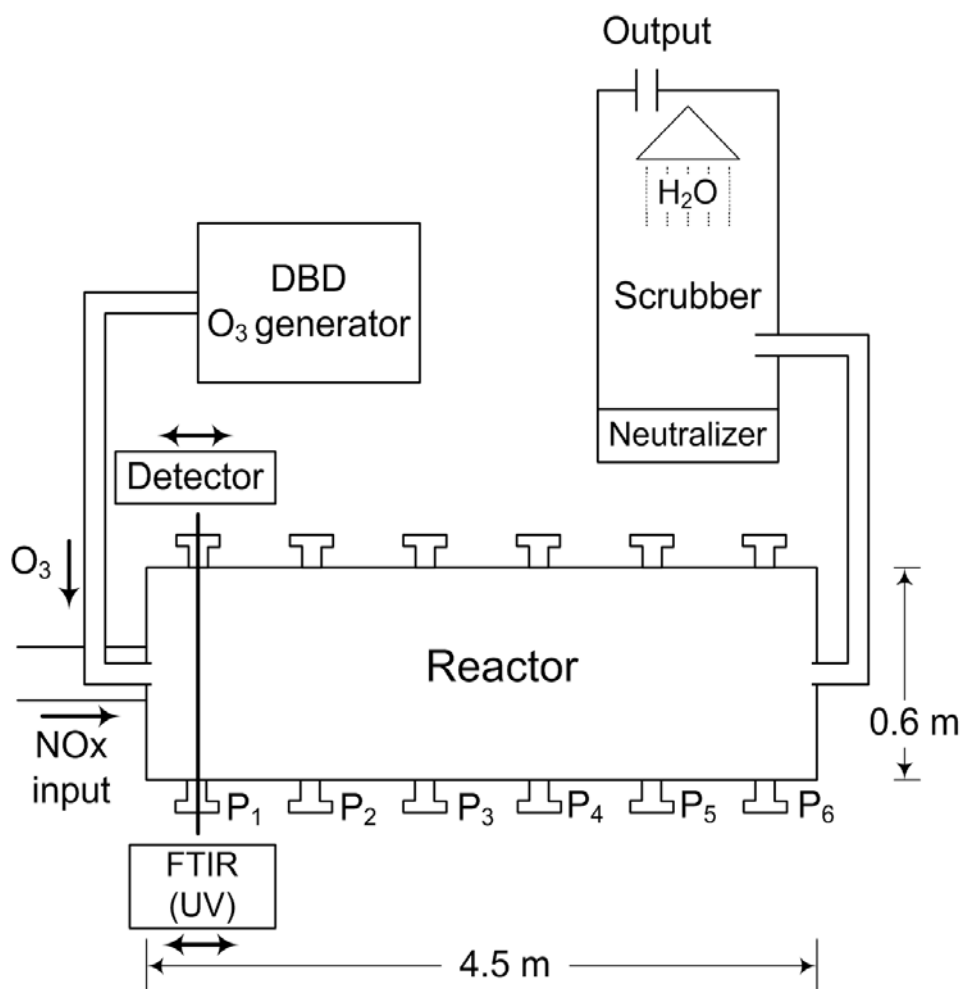


Fig. 2 Schematic of the  $\text{NO}_x$  oxidation process using ozone.

residence time of the flue gas of about 5 seconds was used to oxidize the  $\text{NO}_x$  to soluble  $\text{N}_2\text{O}_5$ . Ozone produced by a Wedeco® generator based on dielectric barrier discharge plasma source operated in  $\text{O}_2$  was injected into the reactor and mixed with the flue gas. A wet scrubber unit was used to capture and neutralize the  $\text{N}_2\text{O}_5$  before releasing the treated gas in the atmosphere. To evaluate the  $\text{NO}_x$  removal efficiency, the input (before the oxidation reactor) and output (after the wet scrubber),  $\text{NO}_x$  concentrations have been measured by a chemiluminescence analyzer (CLD60, Eco

Physics). O<sub>3</sub>, NO<sub>2</sub>, N<sub>2</sub>O<sub>5</sub> and HNO<sub>3</sub> in the reactor were measured by FTIR (MB-100, BOMEM) spectrometer. Ozone concentration was also measured by UV absorption at 254 nm. Six equidistant observation ports (0.87 m) along the reactor were used to detect IR and UV absorption signals. The measurement equipment was placed on a table movable under the reactor, thus keeping the same optical alignment. The following six concentrations of ozone injected into the reactor were used: 1) 25 ppm; 2) 50 ppm; 3) 75 ppm; 4) 100 ppm; 5) 125 ppm; and 6) 150 ppm.

### 2.3 Chemical mechanism of O<sub>3</sub>-NO<sub>x</sub>

Processes influencing on the NO<sub>x</sub> oxidation in the flue gas after the ozone injection were modeled using the chemical kinetics simulation program *CHEMSIMUL*. [16] The program principally consists of a solver of ordinary differential equation (ODE) systems with additional code to transform chemical reaction schemes to ODEs.

### 2.4 Gas phase reactions

Table 1 lists the gas phase reactions included in the model along with the rate constant parameters used in the program. The reaction rate constants are calculated as

$$k = AT^{\beta} e^{-\frac{E_a}{RT}}, \quad (1)$$

where  $R=1.987207 \times 10^{-3} \text{ kcal} \times \text{mol}^{-1} \times \text{K}^{-1}$  is the gas constant,  $E_a$  is the activation energy ( $\text{kcal} \times \text{mol}^{-1}$ ),  $\beta$  is an empirical constant, and  $T$  is the gas temperature. Most of the rate constants in the Table 1 were obtained from the National Institute for Standards and Technology (NIST) kinetic database [17]. In the simulation, all reactions must be treated as bimolecular. For three-body reactions this was achieved by assuming a constant third body density corresponding to an ideal gas at 1 atm., room temperature. In reaction R30, however, the third body concentration was assumed to equal the initial concentration of [H<sub>2</sub>O]. The rate constant of R31 was estimated by an extrapolation from those of R19 and R30 based on the equidistance of the activation energies as calculated by Voegele et al. [18].

ID	Reaction	$A$ ( $\text{cm}^3 \text{ molecule}^{-1} \text{ s}^{-1}$ )	$E_a$ (kcal/mol)	$\beta$	Ref
R1	$\text{NO} + \text{O}_3 \rightarrow \text{NO}_2 + \text{O}_2$ ;	$3.16 \times 10^{-12}$	3.1	0	[1]
R2	$\text{NO}_2 + \text{O}_3 \rightarrow \text{NO}_3 + \text{O}_2$ ;	$1.20 \times 10^{-13}$	4.87	0	[1]
R3	$\text{NO}_2 + \text{NO}_3 \rightarrow \text{N}_2\text{O}_5$ ;	9.42	0	-4.5	[1]
R4	$\text{O}_3 + \text{N}_2 \rightarrow \text{O}_2 + \text{O}(^3\text{P}) + \text{N}_2$ ;	$7.16 \times 10^{-10}$	22.26	0	[1]
R5	$\text{O}(^3\text{P}) + \text{O}_3 \rightarrow 2 \text{O}_2$ ;	$3.11 \times 10^{-14}$	3.14	0.75	[1]
R6	$\text{O}(^3\text{P}) + \text{O}_2 \rightarrow \text{O}_3$ ;	$2.32 \times 10^{-9}$	0	-2.2	[1]
R7	$\text{N}_2\text{O}_5 + \text{N}_2 \rightarrow \text{NO}_2 + \text{NO}_3 + \text{N}_2$ ;	$4.57 \times 10^5$	21.86	-3.5	[1]
R8	$\text{NO}_3 \rightarrow \text{NO} + \text{O}_2$ ;	$2.50 \times 10^6$	12.12	0	[1]
R9	$\text{NO} + \text{O}(^3\text{P}) \rightarrow \text{NO}_2$ ;	$1.51 \times 10^{-6}$	0	-2.41	[1]
R10	$\text{NO}_2 + \text{O}(^3\text{P}) \rightarrow \text{NO}_3$ ;	271	2.29	-4.94	[1]
R11	$\text{NO}_3 + \text{O}(^3\text{P}) \rightarrow \text{O}_2 + \text{NO}_2$ ;	$1.00 \times 10^{-11}$	0	0	[1]
R12	$2 \text{NO}_3 \rightarrow \text{O}_2 + 2 \text{NO}_2$ ;	$8.50 \times 10^{-13}$	4.87	0	[1]
R13	$\text{NO}_2 + \text{NO}_3 \rightarrow \text{O}_2 + \text{NO} + \text{NO}_2$ ;	$5.40 \times 10^{-14}$	2.96	0	[1]
R14	$2 \text{NO}_2 \rightarrow \text{O}_2 + 2 \text{NO}$ ;	$2.71 \times 10^{-12}$	26.03	0	[1]
R15	$2 \text{NO}_2 \rightarrow \text{NO} + \text{NO}_3$ ;	$1.59 \times 10^{-14}$	20.87	0.73	[1]
R16	$2 \text{NO}_2 \rightarrow \text{N}_2\text{O}_4$ ;	0.0259	0	-4.8	[1]
R17	$\text{N}_2\text{O}_4 + \text{H}_2\text{O} \rightarrow \text{HNO}_3 + \text{HNO}_2$ ;	$4.18 \times 10^{-10}$	11.59	0	[1]
R18	$\text{N}_2\text{O}_4 + \text{N}_2 \rightarrow 2 \text{NO}_2 + \text{N}_2$ ;	$3.28 \times 10^4$	12.72	-3.8	[1]
R19	$\text{N}_2\text{O}_5 + \text{H}_2\text{O} \rightarrow 2 \text{HNO}_3$ ;	$2.51 \times 10^{-22}$	0	0	[1]
R20	$\text{HNO}_2 + \text{NO}_3 \rightarrow \text{HNO}_3 + \text{NO}_2$ ;	$1.00 \times 10^{-15}$	0	0	[1]
R21	$\text{NO}_3 + \text{NO} \rightarrow 2 \text{NO}_2$ ;	$1.80 \times 10^{-11}$	-0.22	0	[1]
R22	$\text{O}_3 + \text{NO}_2 \rightarrow \text{NO} + 2 \text{O}_2$ ;	$1.00 \times 10^{-18}$	0	0	[1]
R23	$\text{O}_3 + \text{NO}_3 \rightarrow \text{NO}_2 + 2 \text{O}_2$ ;	$1.00 \times 10^{-17}$	0	0	[1]
R24	$\text{NO} + \text{NO}_3 \rightarrow 2 \text{NO} + \text{O}_2$ ;	$2.71 \times 10^{-11}$	1.882	-0.23	[1]
R25	$2 \text{O}(^3\text{P}) \rightarrow \text{O}_2$ ;	$3.82 \times 10^{-13}$	-1.79	-1	[2]
R26	$\text{O}(^3\text{P}) + \text{NO}_2 \rightarrow \text{O}_2 + \text{NO}$ ;	$5.5 \times 10^{-12}$	0.3736		[2]
R27	$2 \text{NO} + \text{O}_2 \rightarrow 2 \text{NO}_2$ ;	$5.61 \times 10^{-21}$	1.053		[2]
R28	$\text{NO} + \text{NO}_2 \rightarrow \text{N}_2\text{O}_3$ ;	$2.70 \times 10^7$	0	-8.7	[2]
R29	$\text{N}_2\text{O}_3 + \text{N}_2 \rightarrow \text{NO} + \text{NO}_2 + \text{N}_2$ ;	$6.76 \times 10^{14}$	9.7	-8.7	[2]
R30	$\text{N}_2\text{O}_5 + 2 \text{H}_2\text{O} \rightarrow 2 \text{HNO}_3 + \text{H}_2\text{O}$ ;	$4.4 \times 10^{-21}$ (*)			
R31	$\text{N}_2\text{O}_5 + 3 \text{H}_2\text{O} \rightarrow 2 \text{HNO}_3 + 2 \text{H}_2\text{O}$ ;	$8 \times 10^{-20}$ (**)			

(\*) Termolecular reaction; (\*\*) Quadrimolecular reaction.

Table 1. Detailed  $\text{O}_3$  -  $\text{NO}_x$  reaction mechanism.

## 2.5 Heterophase reactions

Three additional, heterophase reactions were included in the model to account for the decomposition of oxygen atoms and ozone on the reaction walls and a possible hydrolysis of  $N_2O_5$  on any water-containing particles in the flue gas.

Reaction R32:

$$\frac{d[O(^3P)]}{dt} = -[O(^3P)] \left( \frac{(30 \text{ cm})^2}{5.78 \times 0.292 \text{ cm}^2 \text{ s}^{-1} (T/273 \text{ K})^{1.5}} + \frac{2 \times 30 \text{ cm}}{9.9 \times 10^{-3} \sqrt{2} \times 4.25 \times 10^4 \text{ cm s}^{-1} \sqrt{T/273 \text{ K}}} \right)^{-1} \quad (2)$$

Reaction R33:

$$\frac{d[O_3]}{dt} = -[O_3] \left( \frac{(30 \text{ cm})^2}{5.78 \times 0.208 \text{ cm}^2 \text{ s}^{-1} (T/273 \text{ K})^{1.57}} + \frac{2 \times 30 \text{ cm}}{2 \times 10^{-6} \sqrt{2} \times 3.47 \times 10^4 \text{ cm s}^{-1} \sqrt{T/273 \text{ K}}} \right)^{-1} \quad (3)$$

## 2.6 Hydrolysis of $N_2O_5$ on droplets

$NO_2$  can be reproduced by  $N_2O_5 \rightarrow NO_2 + NO_3$  back reaction (reaction R7). However this reaction can be suppressed in the presence of a sink for  $N_2O_5$  molecules. One possible sink can be the water droplets from condensation in the reactor. The  $N_2O_5$  uptake by water droplets has been studied by Van Doren *et al.* [19]. They expressed the rate of uptake in terms of an uptake coefficient,  $\gamma_{\text{obs}}$ , which based on their measurements, can be roughly extrapolated to a value of 0.02 for  $N_2O_5$  into water. This coefficient is related to the flux of  $N_2O_5$  into water droplets by  $J = n_g \bar{c} \gamma_{\text{obs}} / 4$ , where  $n_g$  is the gas density ( $[N_2O_5]$ ) and  $\bar{c} = \sqrt{3RT / M_{N_2O_5}} \approx 300 \text{ m/s}$  is the root mean square thermal velocity of the  $N_2O_5$  molecules, which have a molar mass of  $M_{N_2O_5} = 0.108 \text{ kg/mol}$ . Let us assume, for example, that a fraction  $x$  of the  $H_2O$  has condensed and, for simplicity, that spherical droplets of equal radius,  $r$  are formed. The number density of such droplets is  $n_d = n_c / N_d$ , where  $n_c$  is the number density of water molecules that have been condensed into the droplets:

$$n_c = x \cdot [H_2O] = x \cdot C_{H_2O} \cdot \frac{p}{k_B T}, \quad (4)$$

and  $N_d$  is the number of molecules in each such droplet:

$$N_d = \frac{N_A m_d}{M_{H_2O}} = \frac{4N_A \rho \pi r^3}{3M_{H_2O}}, \quad (5)$$

with  $\rho \approx 1 \text{ g/cm}^3$  the density of water,  $M_{H_2O} = 18 \text{ g/mol}$  its molar mass, and  $N_A$  Avogadro's number.

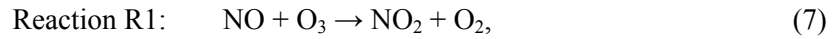
The overall rate of  $N_2O_5$  uptake by these droplets is given by Reaction R34:  $-d[N_2O_5]/dt = JA \equiv \nu_u [N_2O_5]$ , where  $A$  is the total surface area of droplets per unit of vessel volume:

$$A = 4\pi r^2 n_d = \frac{3x \cdot C_{H_2O} \cdot pM_{H_2O}}{\rho r T}. \quad (6)$$

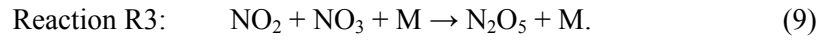
Inserting the above values,  $C_{H_2O}=10\%$ , and  $p=1 \text{ atm}$ , a value for the uptake frequency  $\nu_u$  of  $\sim 0.3 \text{ s}^{-1}$  is found for  $r = 100 \text{ }\mu\text{m}$  and  $\sim 3 \text{ s}^{-1}$  for  $r = 10 \text{ }\mu\text{m}$ . In the present study simulations were performed for both cases: without water droplets and with water droplets of these two drop radii.

## 2.7 Results and discussion

Calculated evolutions of  $O_3$ ,  $NO$ ,  $NO_2$ , and  $N_2O_5$  concentrations in the reactor during 5 seconds after ozone injection are shown in Fig. 3 as an example, at (a) 75 ppm ozone input and (b) 150 ppm ozone input. The kinetic curves in the Fig. 2 were calculated for the  $NO$  initial concentration of 73 ppm and the  $NO_2$  initial concentration of 7 ppm. The simulations in the Fig. 3 do not include any effect of heterophase reactions (Reaction R32, R33, R34). One can see that immediately after ozone injection, the concentration of  $NO$  decreases and the concentration of  $NO_2$  increases accordingly. This is due to the fast reaction



Characteristic time of the  $NO$  conversion to  $NO_2$  depends on the  $O_3$  concentration. Therefore, the first main path of  $NO_x$  reduction is the rapid oxidation of  $NO$  to  $NO_2$  and, later conversion to the  $N_2O_5$  through reactions (8-9) takes place,



The slower process R2 takes place after the process R1 is completed. So, when the input ozone concentration is less than NO concentration, in the first stage the ozone is consumed in  $\text{NO} \rightarrow \text{NO}_2$  conversion without remarkable decrease in  $\text{NO} + \text{NO}_2$

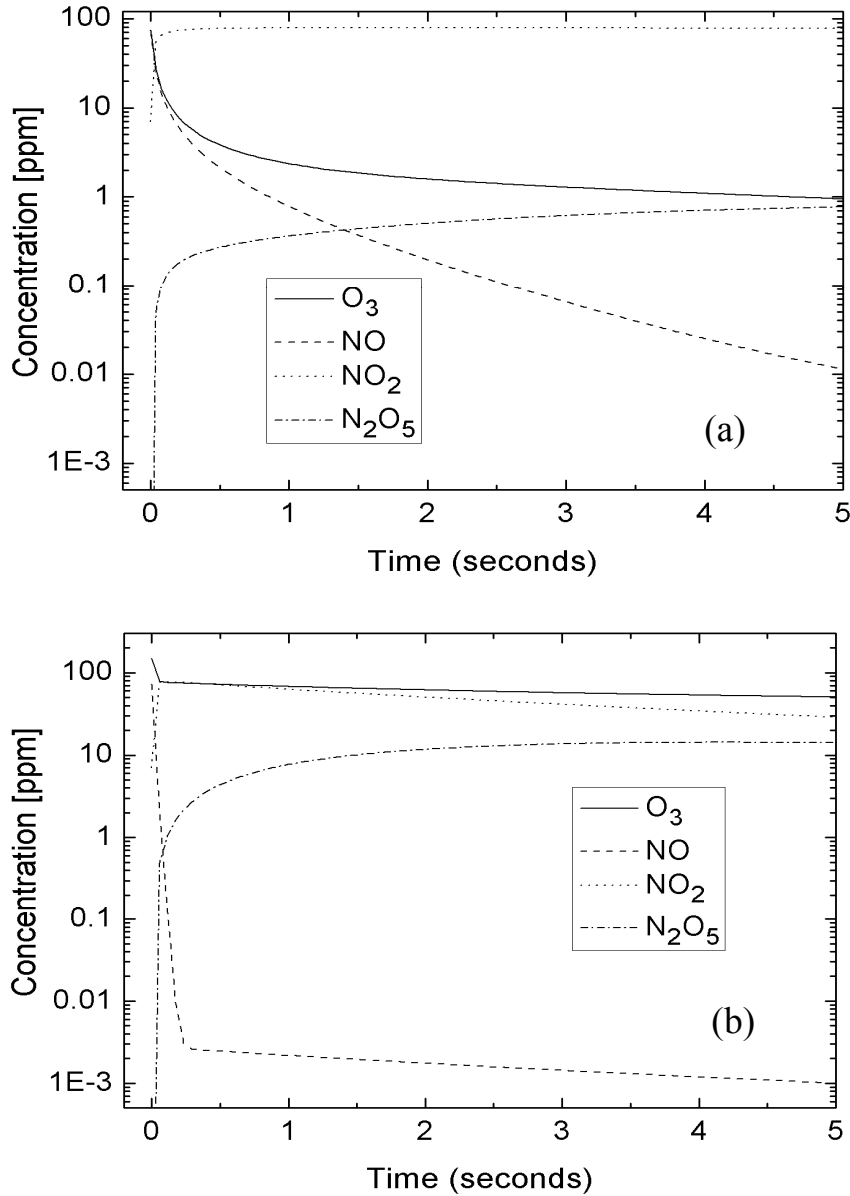
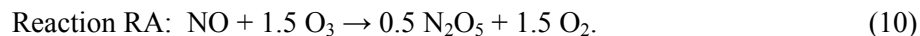


Fig. 3. Calculated evolutions of the concentrations of  $\text{O}_3$ ,  $\text{NO}$ ,  $\text{NO}_2$ ,  $\text{N}_2\text{O}_5$  in the reactor during 5 seconds after ozone injection without considering any effects of heterophase reactions (a) 75 ppm ozone input, (b) 150 ppm ozone input.

concentration as shown in Fig. 3 (a). At higher ozone input level (150 ppm), the conversion of NO to NO<sub>2</sub> is rapid ( $t < 0.3$  seconds) and the excess ozone is used to further oxidize NO<sub>2</sub> (Reaction R2, R3).

The characteristic time of the reaction R2 is determined by the O<sub>3</sub> concentration, as well as the NO<sub>2</sub> concentration determined by reaction R1. For a case when all NO<sub>x</sub> is NO, one can get a deNO<sub>x</sub> reaction path from reactions R1, R2 and R3,



However, when NO<sub>x</sub> is 100 percent by NO<sub>2</sub>, one can get a deNO<sub>x</sub> reaction path from Reaction R2 and R3,

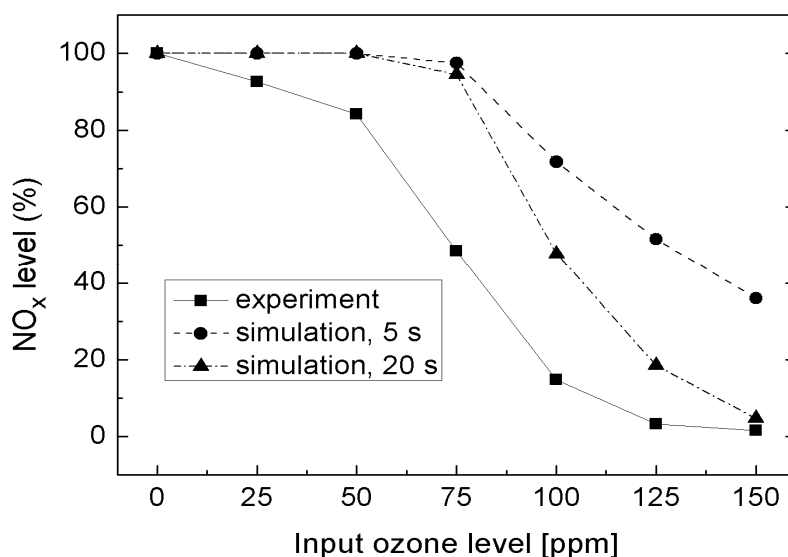


Fig.4 Remained NO<sub>x</sub> after the scrubber at different input ozone level by both experiment measurement and simulations for a residence time of 5 and 20 sec.

This means that if NO is the main component in NO<sub>x</sub>, to remove one NO molecule, 1.5 O<sub>3</sub> molecules are needed, and in the case when NO<sub>2</sub> is the main component in NO<sub>x</sub>, 0.5 O<sub>3</sub> molecules are needed to remove one NO<sub>2</sub> molecule.

Fig. 4 shows the remained NO<sub>x</sub> level after the scrubber at various ozone input levels. The NO<sub>x</sub> reduction efficiency reached 85% for 100 ppm O<sub>3</sub> (molar ratio

$O_3:NO_x = 1.25$ ) and it was higher than 95 % for a 125 ppm input  $O_3$  (molar ratio  $O_3:NO_x = 1.56$ ). In this calculation a residence time of 5 s in the reactor and no wet

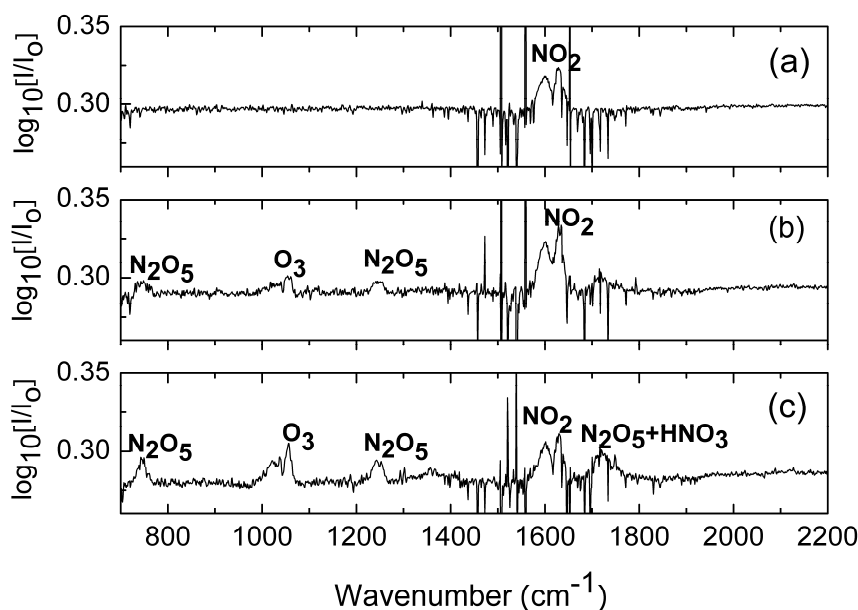


Fig. 5 FTIR absorption spectra measured at  $P_2$  for (a) 25, (b) 100 and (c) 150 ppm ozone input.

scrubbing by water droplets have been assumed.

The spatial distribution of different species was measured by moving the measurement equipment to the various ports. Typical FTIR spectra measured at  $P_2$  port for different ozone input concentrations are shown in Fig. 5. The overlap of water absorption band and NO limits NO detection by FTIR. While the ozone was quickly consumed at lower  $O_3$  inputs (25 ppm and 50 ppm) where no  $O_3$  could be detected by FTIR, the  $NO_2$  peak was the dominant peak. For higher ozone input (150 ppm),  $O_3$ ,  $NO_2$ ,  $N_2O_5$  and  $HNO_3$  were all detected even after about 1 second ( $P_2$ ) after the  $O_3$  injection.

Remained ozone concentration at ports  $P_2$  to  $P_5$  as a function of the ozone input level measured by both FTIR and UV is shown in Fig. 6 for  $NO = 80$  ppm. The  $NO_x$  removal process by ozone oxidation was modeled by solving the rate equations of chemical reactions as listed in the Table 1. Concentrations of different species as a function of the residence time were calculated. Remained ozone levels are shown with dashed lines in Fig. 6 for residence times corresponding to ports  $P_2$  (1 s) and  $P_6$  (5 s). From calculations, it can be seen that for initial ozone concentrations below 80 ppm ( $O_3:NO_x \leq 1$ ), all ozone is consumed for  $NO+NO_2$  oxidation and no ozone remains in the reactor. In the measurements, ozone was



detected for input levels higher than 50 ppm, this may be due to incomplete reaction of ozone in the real situation. With further increase of ozone concentration, the amount of the ozone remained in the reactor increased, however with longer residence time (for example from 1 second or  $P_2$  to 5 seconds or  $P_5$ ) the concentration of the remained ozone decreased. Calculations and experimental

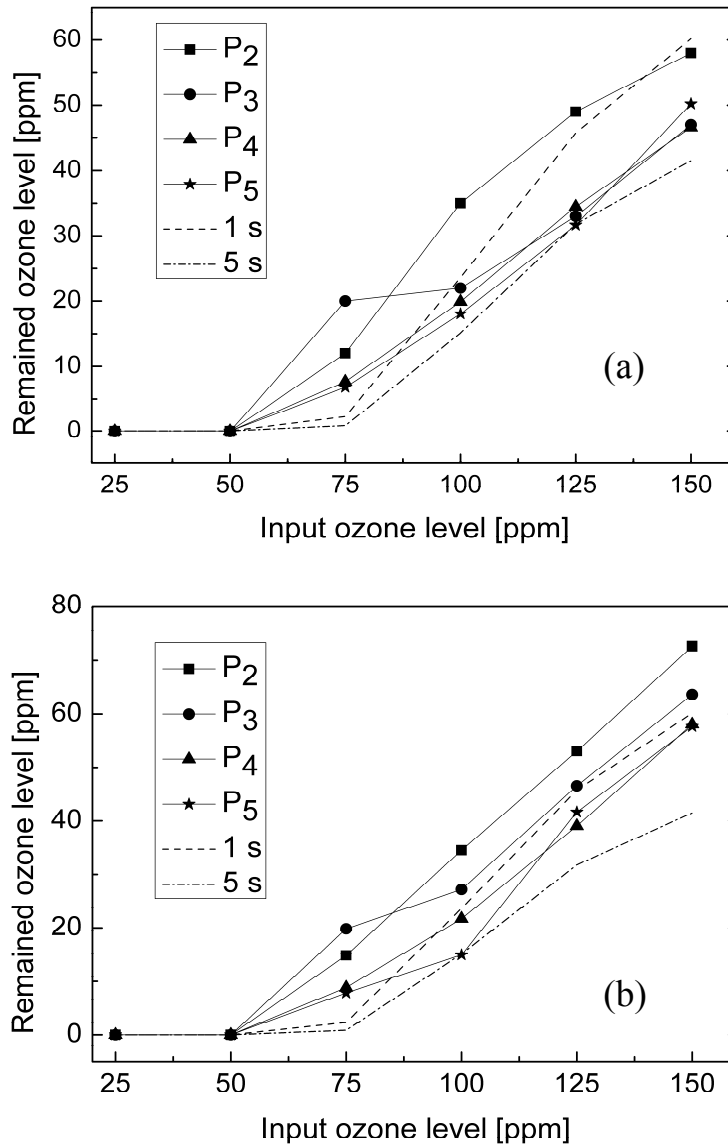


Fig. 6 Ozone concentrations at ports  $P_2$ - $P_5$  as a function of ozone input level measured by (a) FTIR and (b) UV absorption. Dashed lines show the simulated ozone concentration for a residence time of 1 and 5 sec, respectively where,  $NO=80$  ppm and  $T=60$  °C.

results by both FTIR and UV absorption are in good agreement. To achieve high ozone utilization efficiency, long residence time of the flue gas in the reactor is desired. This can be achieved by uniform distribution of the ozone and adequate

mixing of ozone with flue gas and a longer reaction zone.

Simulated  $\text{NO}_2$  and  $\text{N}_2\text{O}_5$  values at different ozone input levels and time after ozone injection with no water sink effect and  $10\ \mu\text{m}$  water droplets in the reactor are shown in Figure 7. The  $\text{NO}_2$  concentration increases with  $\text{O}_3$  input

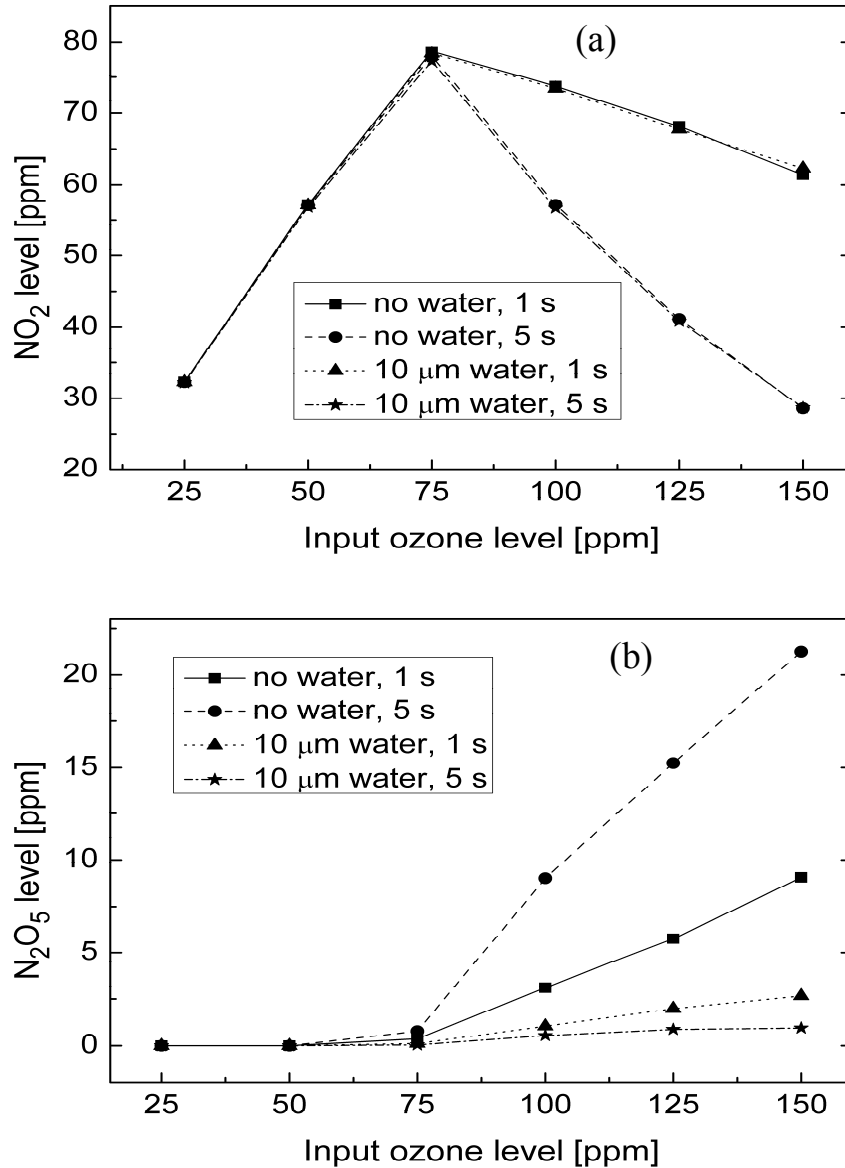


Fig. 7 Simulated  $\text{NO}_2$  (a) and  $\text{N}_2\text{O}_5$  (b) in case of no water in the reactor and  $10\ \mu\text{m}$  water droplets in the reactor for  $T=60\ ^\circ\text{C}$ .

because of  $\text{NO}$  to  $\text{NO}_2$  conversion at low  $\text{O}_3$  input but it decreases for higher  $\text{O}_3$  input due to  $\text{NO}_2$  to  $\text{N}_2\text{O}_5$  conversion. In the case of no water sink effect, the  $\text{N}_2\text{O}_5$  concentration increases with  $\text{O}_3$  input and also with the residence time in the reactor. Without considering water sink effect in simulation, the calculated values for  $\text{N}_2\text{O}_5$  are, as expected, higher than the measured values. However, by taking into

consideration 10  $\mu\text{m}$  water droplets in the reactor, the calculated values for  $\text{N}_2\text{O}_5$  were much lower than the measured values. This suggests that small water droplets have a larger water sink effect on capturing the  $\text{N}_2\text{O}_5$ . Figure 8 presents the  $\text{NO}_2$  (a)

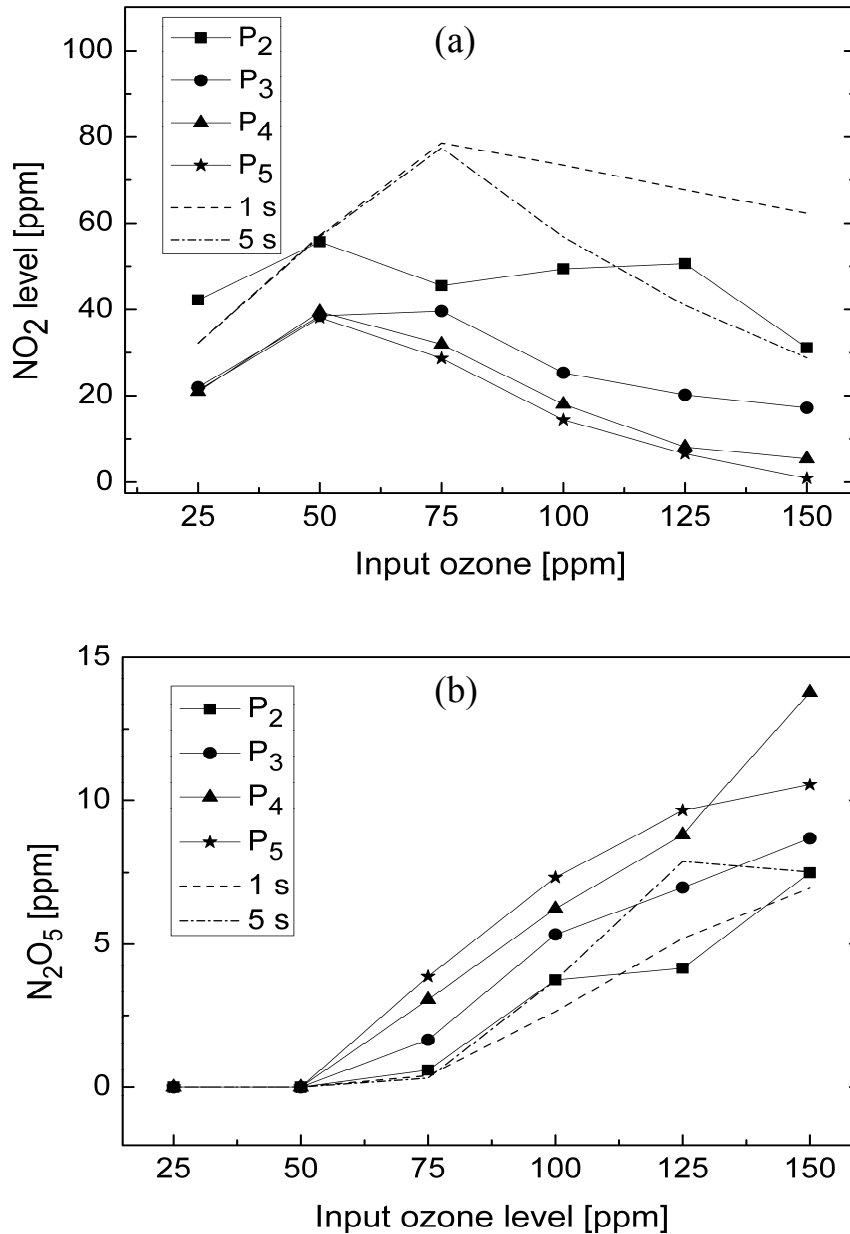


Fig. 8  $\text{NO}_2$  (a) and  $\text{N}_2\text{O}_5$  (b) with simulation considering water sink (100  $\mu\text{m}$  water droplets) effect for  $\text{N}_2\text{O}_5$ , where  $\text{NO}=80$  ppm,  $T=60$   $^\circ\text{C}$ .

and  $\text{N}_2\text{O}_5$  (b) measured concentrations together with simulation considering water sink (100  $\mu\text{m}$  water droplets) effect for  $\text{N}_2\text{O}_5$ . Compared with the case of no water sink effect or the case of 10  $\mu\text{m}$  water droplets in the reactor as shown in the Fig. 7, the calculations in the Fig. 8 shows the best fit correlation with measured values.

It is also interesting to study the effects of flue gas temperature and water capture of  $\text{N}_2\text{O}_5$  on de $\text{NO}_x$  kinetics. Fig. 9 shows calculated concentrations of  $\text{NO}_2$  (a), (a) and (e) and  $\text{N}_2\text{O}_5$  (b), (d) and (f) without considering water sink effect (a) and (b), (c) and (d) considering 100  $\mu\text{m}$  water droplets, and (e) and (f) considering 10  $\mu\text{m}$  water

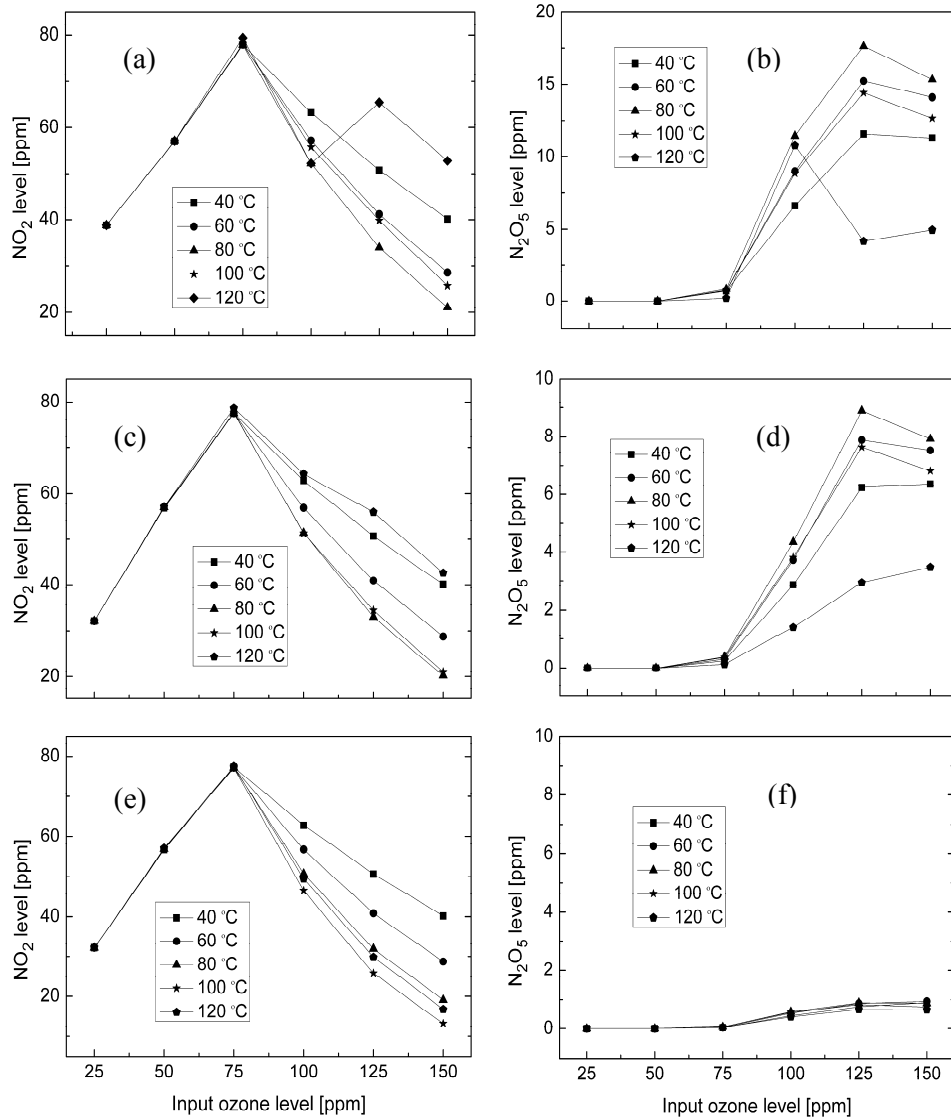


Fig. 9 Temperature dependent concentrations of  $\text{NO}_2$  (a), (c) and (e) and  $\text{N}_2\text{O}_5$  (b), (d) and (f) by calculations (a) and (b) without considering water sink effect for  $\text{N}_2\text{O}_5$ , (c) and (d) considering 100  $\mu\text{m}$  water droplets and (e) and (f) considering 10  $\mu\text{m}$  water droplets (residence time = 5 s,  $\text{NO}=80$  ppm).

droplets for  $\text{N}_2\text{O}_5$  removal at different temperatures within 5 seconds after ozone injection. It shows that in the cases of no water ((a) and (b)) or 100  $\mu\text{m}$  water in the reactor ((c) and (d)), at 80  $^{\circ}\text{C}$  the  $\text{NO}_x$  removal efficiency is the highest (with smallest  $\text{NO}_2$  concentration and highest  $\text{N}_2\text{O}_5$  concentration). The optimum reduction temperature increases to 100  $^{\circ}\text{C}$  in the case considering 10  $\mu\text{m}$  water droplets, Fig. 9

(e). The decomposition rate of ozone (reaction R4:  $O_3 + N_2 \rightarrow O_2 + O(^3P) + N_2$ ) increases at high temperature (over 80 °C) and less ozone is used for NO<sub>x</sub> oxidation. The decomposition of N<sub>2</sub>O<sub>5</sub> (reaction R17:  $N_2O_5 + N_2 \rightarrow NO_2 + NO_3 + N_2$ ) increases also at high temperature (over 80 °C). Thus, one can conclude that the best NO<sub>x</sub> reduction efficiency can be achieved in the order: with 10 µm water droplets, then with 100 µm water and less efficiently with no water. This may be due to the fact that smaller water droplets play a more significant role for N<sub>2</sub>O<sub>5</sub> capture and compete with reaction R17. For example, with an excess of ozone (150 ppm) the NO<sub>x</sub> oxidation efficiency can also be evaluated from the NO<sub>2</sub> concentration in the flue gas. Compare to the case of no water droplets ( Fig. 9 (a)) where NO<sub>2</sub>=21 ppm at 80° C or NO<sub>2</sub>=26 ppm at 100° C, the 10 µm H<sub>2</sub>O (Fig. 8 (e)) droplet content gives improvement in NO<sub>x</sub> oxidation i) from 67.5% to 85% at 100° C or ii) from 73.8 % at 80 °C to 85% at 100 °C. This suggests that the presence of a water spray in the reactor could substantially increase the rate of NO<sub>x</sub> removal. However, it must be noted that it is not obviously desirable to have a mist of nitric acid in the reactor, so the balance of adverse and favorable effects has to be considered carefully.

## ***2.8 Conclusions – gas power plant***

FTIR and UV gas absorption measurements have been performed in a NO<sub>x</sub> oxidation reactor in a large scale experiment where NO<sub>x</sub> was oxidized by plasma-generated O<sub>3</sub>. Reduction rates higher than 95% have been achieved for a molar ratio O<sub>3</sub>:NO<sub>x</sub> = 1.56. A rate equation model has been developed to assess the deNO<sub>x</sub> chemical kinetics in the reactor under various experimental conditions (for example, different flue gas temperatures and humidity). A good agreement was found between measured and calculated values of the main species. Simulation suggests that in current experiment conditions, the deNO<sub>x</sub> efficiency is highest for a flue gas temperature of 100 °C. The addition of small water spray droplets in the reactor may further improve the NO<sub>x</sub> oxidation rate.

## **3 Pilot test measurements in a power plant running on biomass**

### ***3.1 Introduction***

Biomass such as wood and straw are CO<sub>2</sub> neutral fuels which may help to reduce the greenhouse effect. The Danish resources of biomass for the production of energy are estimated to approximate 165PJ a year and only half of which are currently used

[20]. The use of biomass for production of energy is expected to keep an ascendant trend despite of its rather low caloric value. The main pollutants resulting from biofuels are nitrogen, chlorine, potassium and silicon. While potassium and chlorine are deposited on the tubes of the boiler as a salt coating (deposition that can be reduced by silicon) the main emission remains  $\text{NO}_x$ .

The current project also aimed to evaluate the use of the low temperature oxidation by ozone for a biomass power plant both in terms applicability but also for evaluating the  $\text{SO}_x$  and HCl effect on the  $\text{NO}_x$  reduction mechanism.

### 3.2 Chemical kinetics of $\text{NO}_x$ reduction in the presence of $\text{SO}_x$ and HCl

A gas kinetics procedure similar to that presented in paragraph 2.4 was used. The gas phase reactions included in the simulation supplementary to reactions presented in Table 1 are listed in Table 2. The solubility coefficients of  $\text{SO}_2$ ,  $\text{SO}_3$  and HCl in water are, 1.2,  $\infty$  and  $2.5 \times 10^3$ , respectively.

ID	Reaction	$A$ ( $\text{cm}^3 \text{ molecule}^{-1} \text{ s}^{-1}$ )	$E_a$ (kcal/mol)	$\beta$	Ref
R32	$\text{SO} + \text{O}_3 \rightarrow \text{SO}_2 + \text{O}_2$ ;	$4.50 \times 10^{-12}$	2.33	0	[1]
R33	$\text{SO} + \text{O}_2 \rightarrow \text{SO}_2 + \text{O}(3\text{P})$ ;	$1.6 \times 10^{-13}$	4.53	0	[1]
R34	$\text{SO} + \text{O}_2 \rightarrow \text{SO}_3$ ;	$6.1 \times 10^{-21}$	0.543	0	[1]
R35	$\text{SO}_2 + \text{O}_3 \rightarrow \text{SO}_3 + \text{O}_2$ ;	$3.01 \times 10^{-12}$	13.91	0.73	[1]
R36	$\text{SO}_2 + \text{NO}_2 \rightarrow \text{SO}_3 + \text{NO}$ ;	$2 \times 10^{-26}$	0	0	[1]
R37	$\text{SO}_2 + \text{N}_2\text{O}_5 \rightarrow \text{SO}_3 + \text{N}_2\text{O}_4$ ;	$9.1 \times 10^{-24}$	0	0	[1]
R38	$\text{SO}_2 + \text{ClO} \rightarrow \text{SO}_3 + \text{Cl}$ ;	$4 \times 10^{-18}$	0	0	[1]
R39	$\text{SO} + \text{ClO} \rightarrow \text{SO}_2 + \text{Cl}$ ;	$3.22 \times 10^{-11}$	0	0	[1]

Table 2 Main reactions involving  $\text{SO}_x$ .

Calculated evolutions of  $\text{O}_3$ ,  $\text{NO}$ ,  $\text{NO}_2$ ,  $\text{N}_2\text{O}_5$ ,  $\text{SO}$ ,  $\text{SO}_2$  and  $\text{SO}_3$  concentrations in the reactor during 20 seconds after ozone injection are shown in Fig. 10 as an example, for (a) no water and (b) including 10  $\mu\text{m}$  water droplets. The flue gas temperature was set to 115 °C and the input ozone to 500 ppm for a flue gas composition including, 60 ppm of  $\text{SO}_2$ , 140 ppm of  $\text{NO}$ , 10 ppm of  $\text{NO}_2$  and 70 ppm of HCl. The hydrolysis of  $\text{N}_2\text{O}_5$  on droplets was described in a similar way as presented in paragraph 2.6.

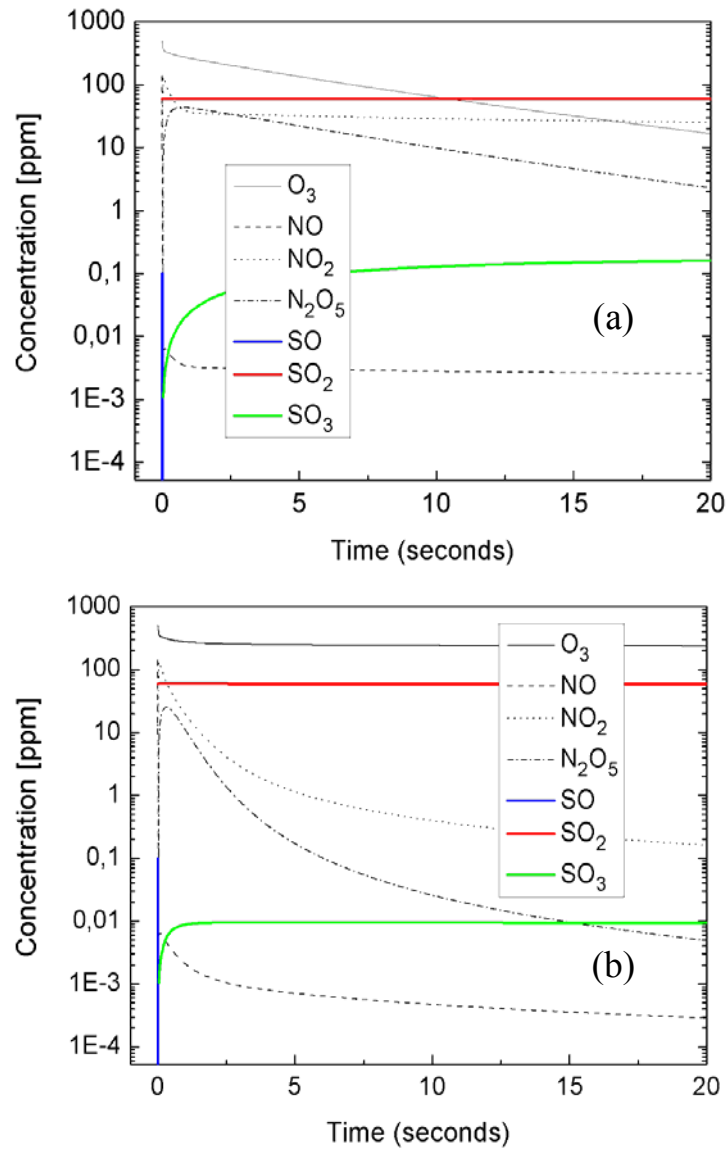


Fig. 10 Calculated evolutions of O<sub>3</sub>, NO, NO<sub>2</sub>, N<sub>2</sub>O<sub>5</sub>, SO, SO<sub>2</sub> and SO<sub>3</sub> concentrations in the reactor during 20 seconds after ozone injection, (a) no water and (b) including 10 μm water droplets.

Since the oxidation rate of SO<sub>2</sub> to SO<sub>3</sub> is too low, due to high  $E_a$  for this reaction, one cannot expect an efficient SO<sub>x</sub> reduction by ozone despite of a good solubility of SO<sub>3</sub> in water. A significant oxidation of SO<sub>2</sub> to SO<sub>3</sub> can only be achieved at temperatures higher than 400°C a value that conflicts with the need to keep the working temperature below 130°C as to prevent the O<sub>3</sub> destruction. Moreover, N<sub>2</sub>O<sub>5</sub> back reaction can also occur at high flue gas temperatures.

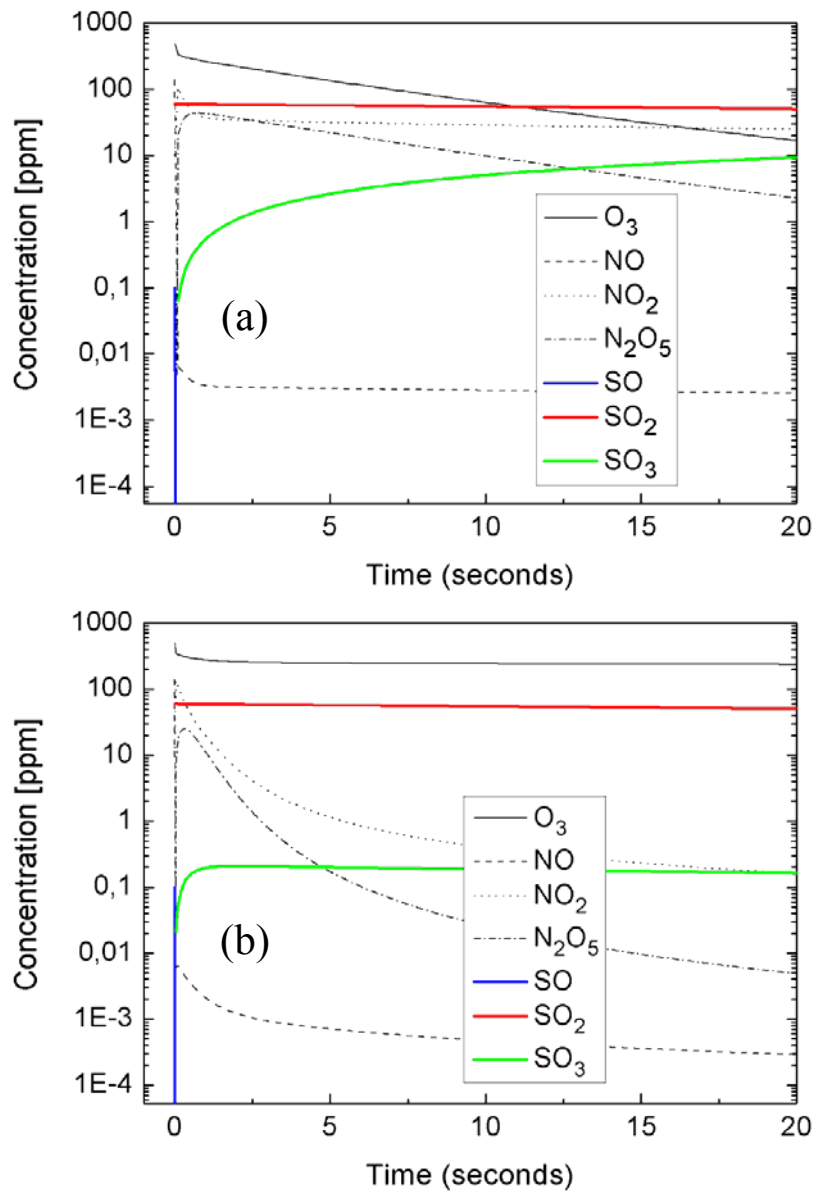


Fig. 11 Calculated evolutions of  $O_3$ ,  $NO$ ,  $NO_2$ ,  $N_2O_5$ ,  $SO$ ,  $SO_2$  and  $SO_3$  concentrations in the reactor during 20 seconds after ozone and COI injection (100 ppm) (a) no water and (b) including 10  $\mu m$  water droplets.

The evolution of simulated concentrations of different radicals in the presence of 100 ppm of ClO is presented in Fig. 11 (a) with no water and (b) with 10  $\mu m$  water droplets. The other input concentrations are similar with those used in Fig. 10. Except for the effect on water droplets on  $H_2O_5$  the simulation shows that ClO will have very limited influence on  $NO_x$  and  $SO_x$  reduction.



One alternative would be to remove simultaneously SO<sub>2</sub> and NO by wet scrubbing using chlorine dioxide solution [21]. HCl can also be removed by wet scrubbing as shown in the following reaction,



### 3.3 Experimental details – Haslev

The following aspects were significantly different from the measurements performed at the power plant running on natural gas in Ringsted:

- The flue gas temperature was around 115 °C (only 60° C at Ringsted);
- The NO<sub>x</sub> level was strongly fluctuating in time, in a range from 100 ppm up to 300 ppm (the NO<sub>x</sub> level in Ringsted was almost constant at 80 ppm);
- The inner pressure in the reactor was positive (slightly negative at Ringsted);
- Higher water vapor concentrations;
- Large content of dust particles (almost dust free combustion at Ringsted).

All these aspects needed special care for the measurement system that was severely affected by water condensation and deposition of large dust particles on the observation windows as shown in Fig. 12 (a). In order to avoid these problems the windows were flashed all the time with a low flow of dry air as shown in Fig. 12 (b).



Fig 12 (a) Measurement windows contaminated with large dust particles; (b) Mounting system for observation window including a small pipe for pouring dry air.

### 3.4 Experimental results and discussion

Three traces of the NO<sub>x</sub> level recorded continuously for 15 min at time intervals larger than several hours are shown in Fig. 13. As one can see, due to unavoidable unsteady combustion of the straw, the NO<sub>x</sub> level was fluctuating most of the time with variations larger than 100 ppm in less than one minute.

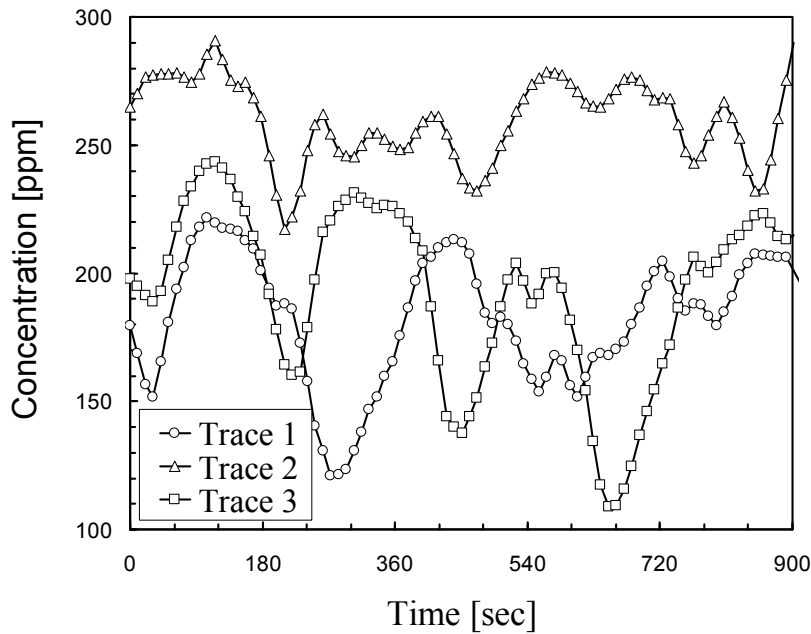


Fig. 13 Typical NO<sub>x</sub> levels as a function of time for a biomass power plant, showing very large variation within one minute time interval.

The NO<sub>x</sub> levels measured at the input, NO<sub>x</sub>\_In, and output, NO<sub>x</sub>\_Out, of the reactor with the corresponding level of ozone after the oxidation process took place, Ozone\_Out, are shown in Fig. 14 for a constant input of ozone of (a) 300 g/h and (b) 500 g/h. While a NO<sub>x</sub> reduction rate of about 50% resulted in large amounts of unused ozone correlated with low NO<sub>x</sub> levels at that particular time, a NO<sub>x</sub> reduction rate larger than 80% resulted in amounts of unused ozone that are unaffordable taking into consideration that the operation cost is mainly reflected in the price of the ozone.

In order to solve the problem of a time dependent NO<sub>x</sub> level for biomass power plants a special NO<sub>x</sub> reduction scheme was implemented. The main idea is that one can minimize the ozone loss by correlating the ozone and NO<sub>x</sub> levels at the input of the reactor. Since the ozone generator has an internal reaction time to deliver and transport a requested amount of ozone,  $\Delta T_{O_3}$ , the optimization scheme can not be implemented as a direct feedback between the NO<sub>x</sub> level at the input of the reactor and the command signal of the ozone generator. For example, the reaction time for the ozone generator used in this project is shown in Fig. 15, where the requested ozone level was incremented with 100 g/h by 3 minutes time intervals.

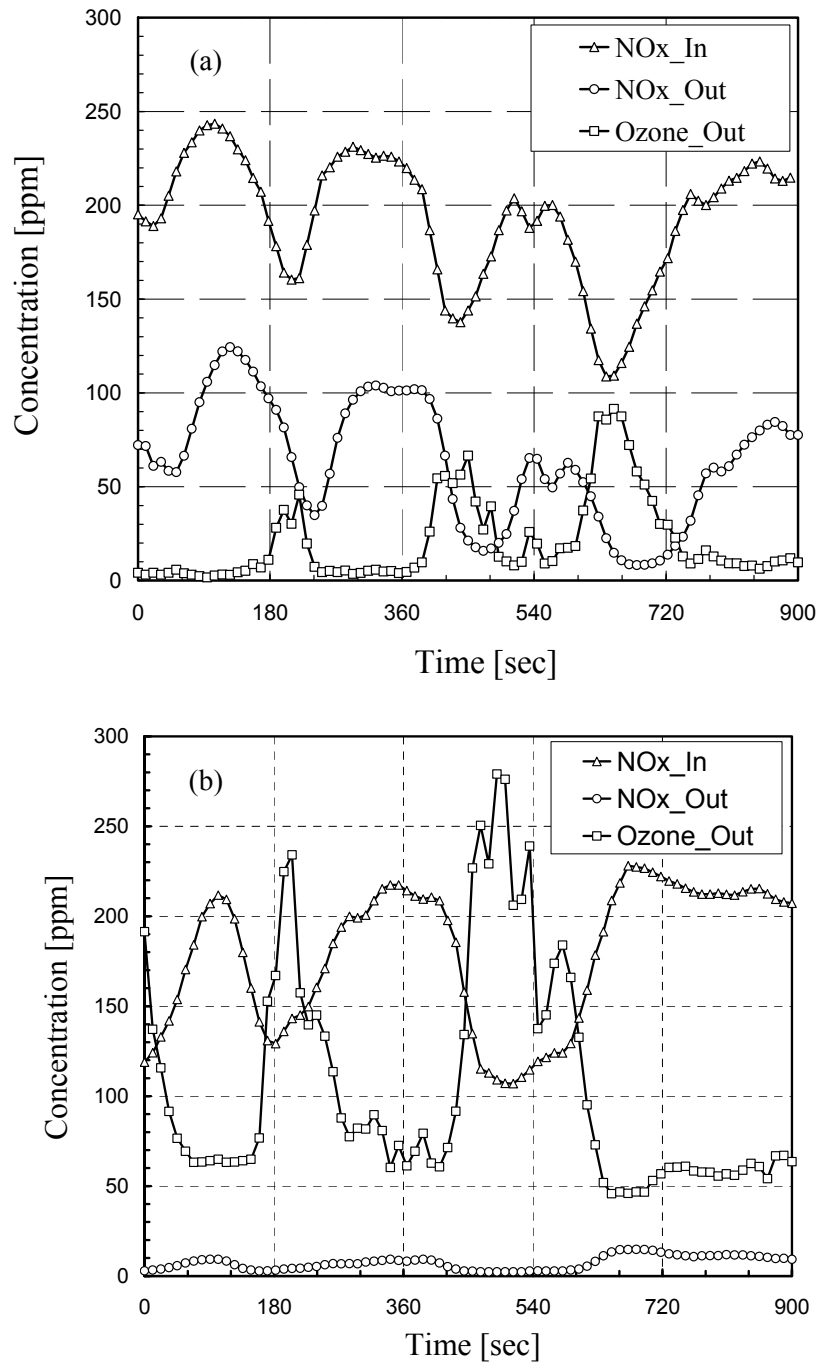


Fig. 14 NO<sub>x</sub> levels at the input and output of the reactor with the corresponding unconsumed ozone for a constant input of ozone of (a) 300 g/h and (b) 500 g/h.

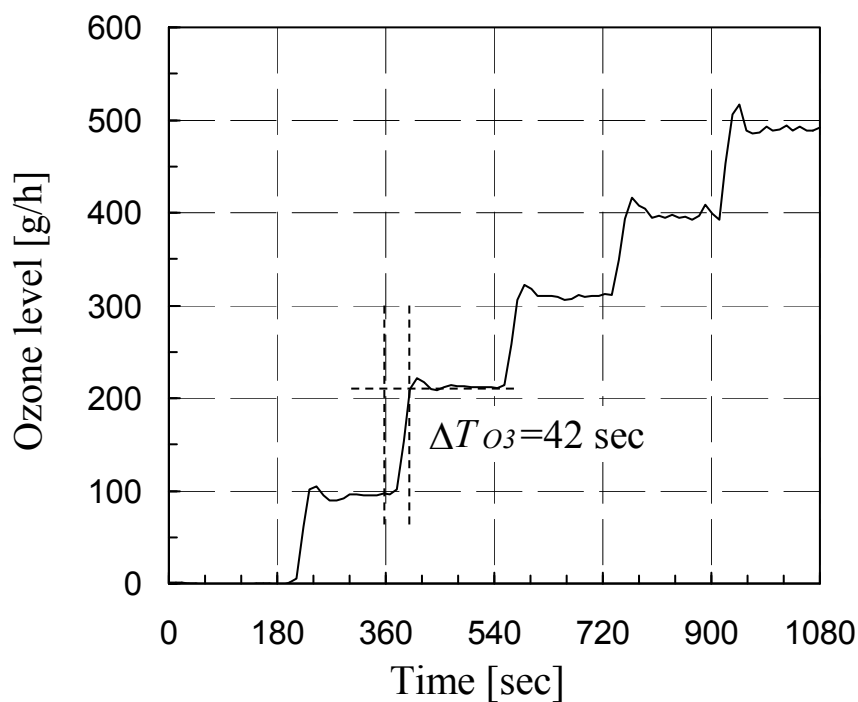


Fig. 15 Ozone levels showing an almost constant generation and transport time of about 42 seconds without respect of the delivered concentration. The ozone generator was set to change its output at equal time intervals of exactly 3 min.

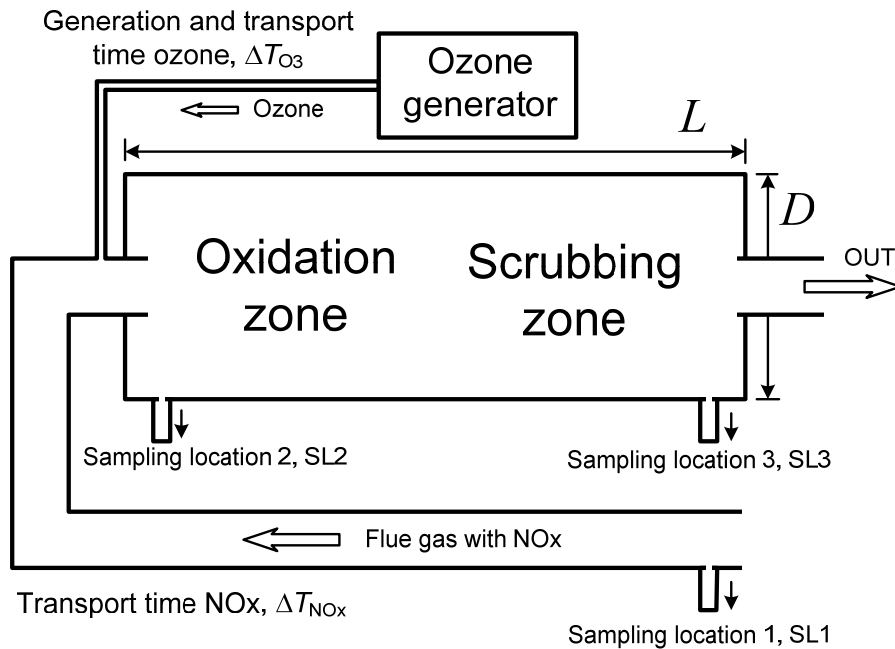


Fig. 16 Schematic of the optimization scheme.  $\text{NO}_x$  is sampled at locations SL1, SL2 and SL3 while ozone at SL2 and SL3.

This measurement shows that the generator needed about 42 seconds to adjust the ozone level to the requested value and to transport it to the entrance of the reactor. For an optimum match between the NO<sub>x</sub> and ozone levels one needs to know the NO<sub>x</sub> level more than 42 sec prior to the flue gas entrance in the reactor.

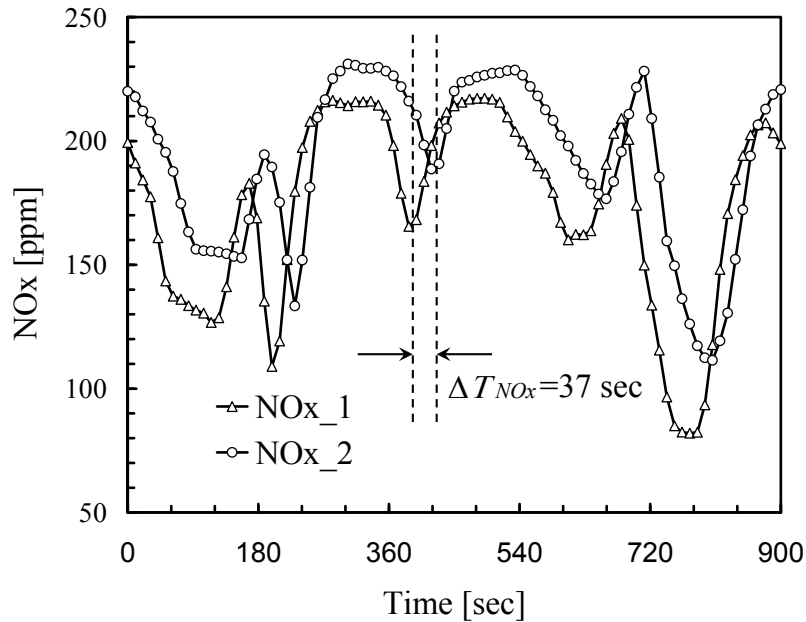


Fig. 17 NO<sub>x</sub> levels at two locations, 1 and 2, showing that a transportation line of 25 m between provides a time delay of 37 seconds. The 10 % difference in the NO<sub>x</sub> levels is attributed to different sensor calibration.

The implementation of such an optimization principle is shown in Fig. 16 where the oxidation and the scrubbing zones are merged schematically. SL1, SL2 and SL3 are three sampling locations where the NO<sub>x</sub> level can be measured while the ozone level is measured only at SL2 and SL3. If  $\Delta T_{NOx}$  is the transport time between SL1 and SL2 then one needs a geometric distance of about 35 m to compensate  $\Delta T_{O_3}$  at a gas flow of 0.9 m/sec. Since most of the power plants are using rather long evacuation lines for the flue gas, including portions of heat exchange, it makes possible to ensure  $\Delta T_{NOx}$  time intervals of more than 20 seconds by placing a NO<sub>x</sub> sensor as close as possible to the combustion zone.

The NO<sub>x</sub> level measured at two locations situated about 25 m apart is shown in Fig. 17 from where one can deduce a transport time of 37 sec. The 10% difference in the NO<sub>x</sub> levels can be the result of different calibration between the power plant sensor and DGC's NO<sub>x</sub> detection system. The very good correlation between the shapes of the two signals proves that one can use the NO<sub>x</sub> level measured at a location prior the reactor entrance to compensate the reaction and transport time for

ozone. In practice the ozone generator can be placed just a few meters from the oxidation reactor, so that it is possible to assume that the  $\Delta T_{O_3}$  is mainly the reaction time of the generator.

In order to test this optimization scheme the rental time for the equipment was extended with two weeks. However, this time interval was not enough for a complete implementation, so that, the optimization scheme was implemented only partially in the sense that we could compensate only time fluctuations larger than one 30 sec.

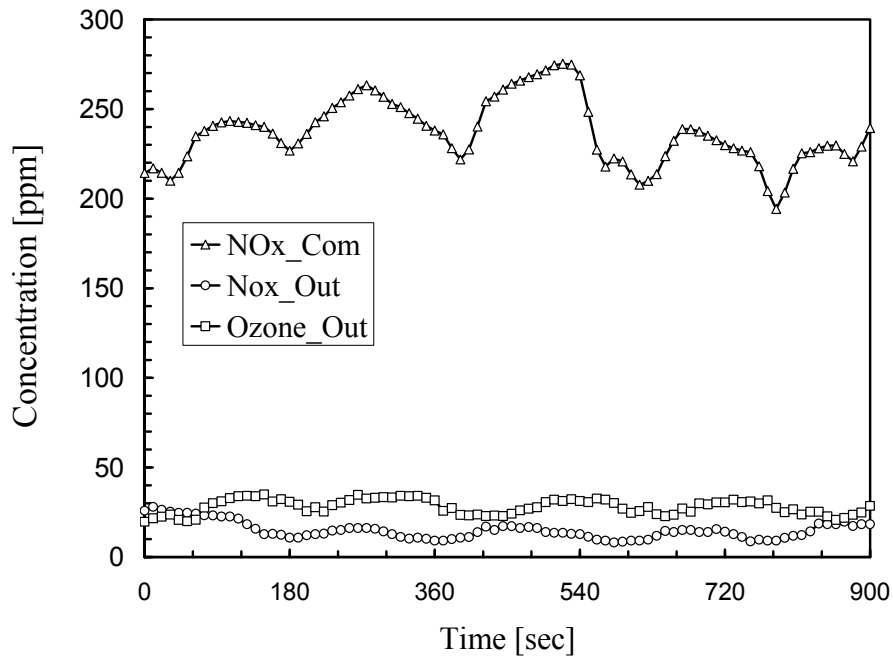


Fig. 18 NO<sub>x</sub> level commanding the ozone generator, NO<sub>x</sub>\_Com, and NO<sub>x</sub> and ozone levels after the scrubber, NO<sub>x</sub>\_Out and Ozone\_Out, respectively.

Fig. 18 presents with NO<sub>x</sub>\_Com the NO<sub>x</sub> level used to command the ozone level in the ozone generator, and NO<sub>x</sub>\_OUT and Ozone\_OUT the NO<sub>x</sub> and ozone levels after the scrubber. A NO<sub>x</sub> reduction rate higher than 85% obtained at the same time with a low level of unconsumed ozone proves the applicability of this new optimization scheme which was not previously used in research or direct implementations for NO<sub>x</sub> reduction by ozone oxidation.

### 3.5 Conclusions – biomass power plant

NO<sub>x</sub> reduction by ozone oxidation is applicable for biomass power plants. However, due to large fluctuations in the NO<sub>x</sub> level within time intervals of a few minutes a special optimization scheme ensuring an efficient use of ozone is required. Such

optimization has been developed and partially implemented. The oxidation rate of SO<sub>2</sub> to soluble SO<sub>3</sub> by ozone is too low at temperatures below 130 °C. Higher operation temperatures are not applicable due to significant ozone destruction. SO<sub>x</sub> and HCl have a very small effect on NO<sub>x</sub> reduction by ozone.

#### 4 References

- [1] Orlandini I and Riedel U, J Phy. D: Appl Phys 2000;33:2467-2474.
- [2] Chen J P and Yang R T, Appl Catal A 1992;80:135-148.
- [3] Lyon R K, US Patent No. 3900554 (1975).
- [4] Nam C M, Gibbs B M, Proc Combust Inst 2000;28:1203-9.
- [5] Jarvis J B, Naresh A T D, Suchak J, LoTO<sub>x</sub> process flexibility and multi-pollutant control capability. Presented at the combined power plant air pollutant control mega symposium, Washington, DC, May 19-22, 2003.
- [6] Mukkavilli S, Lee C K, Varghese K, and Tavlarides L L, IEEE Trans Plasma Sci 1988;16:652-660.
- [7] Dinelli G, Civitano L, and Rea M, IEEE Trans Ind Appl 1990;26:535-541.
- [8] Chakrabarti A, Mizuno A, Shimizu K, Massuoka T, and Furuta S, IEEE Trans Ind Appl 1995;31:500-6.
- [9] Yamamoto T, Yang C L, Kravets Z, and Kravets M, IEEE Trans Ind Appl 2000;36:923-7.
- [10] Chang S J, Loay P C, Nagai K, Yoshioka T, Aoki S, Moezawa A, IEEE Trans Ind Appl 1996;32:131-7.
- [11] Martin D I, Ighigeanu D I, Mateescu E N, Craciun G D, Calinescu I I, Iovu H M, and Marin G G, IEEE Trans Ind Appl 2004;40:41-52.
- [12] Ferrel R, Pollut. Engr. 2000;32:50-3.
- [13] Yoshioka Y, Sano K and Teshima K, J Adv Oxid Technol 2003;6:143-9.
- [14] Eliasson B and Kogelschatz U, IEEE Trans Plasma Sci 1991;19:309-323.
- [15] Using Non-Thermal Plasma to control air pollutants, Report EPA-456/R-05-001 United States Environmental Protection Agency, Feb. 2005  
<http://www.epa.gov/ttn/catc/dir1/fnonthrm.pdf>
- [16] Kirkegaard P, Bjergbakke E, and Olsen J V, *Risø-R-1085 (ed.2) (EN)*, 1 (2006).
- [17] NIST database, <http://kinetics.nist.gov/>
- [18] Voegelé A F, Tautermann CS, Loerting T, and Liedl K R, Phys.Chem.Chem.Phys. 2003;5:487-495.
- [19] Van Doren J M, Watson L R, Davidovits P, Worsnop D R, Zahniser M S, and Kolb C E J Phys Chem 1990;94:3265-69.

- [20] Bioenergy for electricity and heat – experiences from biomass-fired CHP plants in Denmark, published by DONG Energy, 2007
- [21] D.S. Jin et al., *Journal of Hazardous Materials B* 135 (2006) 412.



Risø DTU is the National Laboratory for Sustainable Energy. Our research focuses on development of energy technologies and systems with minimal effect on climate, and contributes to innovation, education and policy. Risø has large experimental facilities and interdisciplinary research environments, and includes the national centre for nuclear technologies.

---

**Risø DTU**  
**National Laboratory for Sustainable Energy**  
**Technical University of Denmark**

Frederiksborgvej 399  
PO Box 49  
DK-4000 Roskilde  
Denmark  
Phone +45 4677 4677  
Fax +45 4677 5688

[www.risoe.dtu.dk](http://www.risoe.dtu.dk)